Implantable multireservoir device with stimulus-responsive membrane for on-demand and pulsatile delivery of growth hormone

Seung Ho Lee[a,b,1], Huiyan Piao[c,1], Yong Chan Cho[d], Se-Na Kim[d], Goeun Choi[e], Cho Rim Kim[d], Han Bi Ji[d], Chun Gwon Park[f], Cheol Lee[g], Chong In Shin[h], Won-Gun Koh[i], Young Bin Choy[b,d,h,2], and Jin-Ho Choy[c,e,j,2]

[a]Institute of Nano-Science and Nano-Technology, Yonsei University, Seoul 03722, Republic of Korea; [b]Institute of Medical and Biological Engineering, Medical Research Center, Seoul National University, Seoul 03080, Republic of Korea; [c]Center for Intelligent Nano-Bio Materials (CINBM), Department of Chemistry and Nanoscience, Ewha Womans University, Seoul 03760, Republic of Korea; [d]Interdisciplinary Program in Bioengineering, College of Engineering, Seoul National University, Seoul 08826, Republic of Korea; [e]Intelligent Nanohybrid Materials Laboratory (INML), Institute of Tissue Regeneration Engineering (ITREN), Dankook University, Cheonan 31116, Republic of Korea; [f]Department of Biomedical Engineering, SKKU Institute for Convergence, Sungkyunkwan University (SKKU), Suwon 16419, Republic of Korea; [g]Department of Pathology, Seoul National University College of Medicine, Seoul 03080, Republic of Korea; [h]Department of Biomedical Engineering, Seoul National University College of Medicine, Seoul 03080, Republic of Korea; [i]Department of Chemical and Biomolecular Engineering, Yonsei University, Seoul 03722, Republic of Korea; and [j]Tokyo Tech World Research Hub Initiative (WRHI), Institute of Innovative Research, Tokyo Institute of Technology, Yokohama 226-8503, Japan

Edited by Robert Langer, Massachusetts Institute of Technology, Cambridge, MA, and approved May 3, 2019 (received for review April 30, 2019)

Implantable devices for on-demand and pulsatile drug delivery have attracted considerable attention; however, many devices in clinical use are embedded with the electronic units and battery inside, hence making them large and heavy for implantation. Therefore, we propose an implantable device with multiple drug reservoirs capped with a stimulus-responsive membrane (SRM) for on-demand and pulsatile drug delivery. The SRM is made of thermosensitive POSS(MEO_2MA-co-OEGMA) and photothermal nanoparticles of reduced graphene oxide (rGO), and each of the drug reservoirs is filled with the same amount of human growth hormone (hGH). Therefore, with noninvasive near-infrared (NIR) irradiation from the outside skin, the rGO nanoparticles generate heat to rupture the SRM in the implanted device, which can open a single selected drug reservoir to release hGH. Therefore, the device herein is shown to release hGH reproducibly only at the times of NIR irradiation without drug leakage during no irradiation. When implanted in rats with growth hormone deficiency and irradiated with an NIR light from the outside skin, the device exhibits profiles of hGH and IGF1 plasma concentrations, as well as body weight change, similar to those in animals treated with conventional s.c. hGH injections.

drug delivery | implantable device | near-infrared light | stimulus-responsive membrane

Implantable drug delivery systems enabled with on-demand drug delivery have attracted considerable attention for the treatment of chronic diseases requiring long-term drug therapy (1, 2). Such systems are considered advantageous in that, after one-time implantation, complex drug regimens could still be achieved without a conventional means of drug administration, such as multiple invasive injections (3). To release drugs only at the desired times, many implantable devices were designed to contain the driving and controller units (4–13), and thus they became large and heavy, which could be inconvenient from the perspective of patient compliance.

In this regard, implantable devices that can release drugs via an external stimulus have been extensively studied in recent years (14–17). Those devices were composed mainly of the drug reservoirs without any additional driving units inside, and the reservoir was capped with a membrane, the shape or permeability of which could be changed upon applications of a noninvasive stimulus applied from the outside skin to trigger the onset of drug release (14–17). However, the membrane was not yet properly optimized for the regimen of the drugs that especially need a pulsatile delivery to follow circadian rhythm (18, 19). For example, the change of membrane property was very slow, causing delayed or prolonged drug release (14–17). The pores or apertures present in the membrane could cause continuous drug leakage even without the presence of stimuli (15, 17).

Therefore, we propose an implantable device with multiple drug reservoirs capped with a stimulus-responsive membrane (SRM) specifically for on-demand and pulsatile drug delivery. For this purpose, we employed a continuous-wave near-infrared (NIR) light at wavelength of 808 nm as a noninvasive means of stimulus, which possesses a high permeability in soft tissues without damage (20–22). We prepared the SRM as a thermosensitive polymer hybrid composed of POSS(MEO_2MA-co-OEGMA) and nanoparticles of reduced graphene oxide (rGO). Therefore, each reservoir was seamlessly capped with this SRM to prevent drug leakage during the off-states. Only when an NIR light was irradiated would the rGO nanoparticles in the membrane generate heat (22–24), which in turn would shrink the thermosensitive polymer, letting it be torn (25), leading to rupture of the membrane and hence the onset of drug release. The POSS(MEO_2MA-co-OEGMA) and rGO herein are known to be biocompatible, and thus they have been used for many other biomedical applications (26, 27).

To test the feasibility of the device herein, we loaded it with human growth hormone (hGH), as hGH is often prescribed for

Significance

We propose an implantable multireservoir device equipped with stimulus-responsive membrane to allow for on-demand and pulsatile drug delivery. The stimulus-responsive membrane is made of a thermosensitive polymer, POSS(MEO_2MA-co-OEGMA), and photothermal nanoparticles of reduced graphene oxide. Each of the drug reservoirs is filled with the same amount of human growth hormone and capped with the stimulus-responsive membrane. Therefore, when implanted in living animals, the device herein can deliver drug reproducibly by rupturing a stimulus-responsive membrane only at the times of near-infrared irradiation applied from the outside body without showing complications.

Author contributions: S.H.L., H.P., Y.B.C., and J.-H.C. designed research; S.H.L., H.P., Y.C.C., S.-N.K., C.R.K., H.B.J., and C.I.S. performed research; J.-H.C. contributed new reagents/analytic tools; G.C., C.G.P., and C.L. analyzed data; and S.H.L., H.P., W.-G.K., Y.B.C., and J.-H.C. wrote the paper.

The authors declare no conflict of interest.

This article is a PNAS Direct Submission.

[1]S.H.L. and H.P. contributed equally to this work.

[2]To whom correspondence may be addressed. Email: ybchoy@snu.ac.kr or jhchoy@dankook.ac.kr.

This article contains supporting information online at www.pnas.org/lookup/suppl/doi:10.1073/pnas.1906931116/-/DCSupplemental.

Published online May 23, 2019.

on-demand and pulsatile delivery via injections for treatment of growth hormone deficiency in clinical settings (28). The performance of the device was tested under in vitro environments, where the SRM on a selected reservoir was irradiated with NIR light only at scheduled times while the device was immersed in PBS (pH 7.4) at 37 °C for 28 d. For in vivo evaluation, the device was implanted in living animals with growth hormone deficiency, i.e., hypophysectomized rats, and the pharmacokinetic and pharmacodynamic profiles were evaluated while the device was irradiated every day for 14 d.

Results

Implantable Device Preparation and Operation. We prepared the device to contain 18 distinct drug reservoirs as a prototype, as shown in Fig. 1*A*. For this, we prepared three distinct constituent parts of the top cover, drug reservoir body, and bottom cover, each of which was fabricated with a PolyJet 3D printer (Eden 350V; Objet Geometries) using polyurethane copolymer. We then assembled and attached those parts with medical epoxy (Epo-Tek 301; Epoxy Technology) to produce the device herein. In this work, the whole surface of the device was coated with Parylene C to promote the biocompatibility of the device after implantation (29). Detailed fabrication procedures are depicted in *Materials and Methods* and *SI Appendix*, Fig. S1.

The drug reservoir body was shaped to contain 18 hollow cylinders, the top of which was seamlessly sealed with the SRM prepared in this work, using medical epoxy. Then, each drug reservoir was filled with recombinant hGH (EutropinPEN; 36 IU; LG Chemical), followed by polyethylene glycol (PEG) (MW 400; Acros Organics), to give a loading amount of 20.01 ± 0.43 μg of hGH per reservoir [hGH:PEG = 1:1.13 (wt/wt)]. Then, the bottom was seamlessly sealed with a polyester tape (Ideal 9144 tape; American Biltrite). The drug reservoir body was glued with the top cover, which contained 18 openings that were aligned to just expose the SRM on each of the corresponding drug reservoirs. Finally, the bottom cover was glued with medical epoxy to produce the device.

We also prepared the external guide for the purpose of alignment of the NIR irradiation from the outside body. The device and external guide were each embedded with two magnets of opposite polarity in a way that the magnets in the external guide could be attracted and attached to those in the implanted device with directionality. Thus, each of the hollow cylinders in the external guide could be aligned to the SRM on a specific drug reservoir, where the tip of the NIR laser (OCLA; Soodogroup) could be inserted for irradiation. To be able to recognize an already used reservoir, the top of the external guide was covered with a thin film of polypropylene (CCR 50; CAS Chemical), which could be punctured when the tip of the NIR laser was applied.

Therefore, the device herein could be operated as follows (Fig. 1*B* and Movie S1): (*i*) the external guide at the outside skin could be attached to the implanted device for alignment; (*ii*) the NIR laser was irradiated through a selected cylinder in the external guide; (*iii*) the SRM on a selected drug reservoir was ruptured and opened; and (*iv*) the hGH was released. Fig. 1*C* shows the optical images of the device and external guide prepared in this work. The device had dimensions of ∼24 mm × 9 mm × 5 mm [length (L) × width (W) × height (H)], giving a total volume of ∼1 mL. Each drug reservoir was shaped to be 1.5 mm in diameter with a height of 3.5 mm, giving a volume of ∼6.2 μL. The external guide had a dimension of 27 mm × 11.5 mm × 9.5 mm (L × W × H), giving a total volume of ∼3 mL (Fig. 1*C*).

SRM Ruptured via NIR Irradiation. To deliver hGH in on-demand and pulsatile manners, we prepared the SRM to be able to rupture and open the drug reservoir via NIR irradiation. Thus, the SRM consisted mainly of a thermosensitive polymer, POSS(MEO_2MA-co-OEGMA), which shrinks in response to heat, i.e., an increase in temperature, due to the break of hydrogen bonds above the lower critical solution temperature (LCST) (26). To allow for heat generation via NIR irradiation, the membrane was prepared in the form of a composite to contain the nanoparticles of rGO, which possesses an effective photothermal property (25). The energy absorbed by the photoactivated rGO can be quickly transferred to that of molecular vibration, which is finally converted into thermal energy due to the delocalized electrons. Therefore, the chains of POSS(MEO_2MA-co-OEGMA) would collapse and form the large aggregates when the temperature increased by the NIR-irradiated rGO nanoparticles.

In this work, we aimed to prepare the SRM to be relatively rapidly ruptured with NIR irradiation (5 s). For optimization, therefore, we prepared the SRM with three different contents of the rGO nanoparticles: 0 wt% (i.e., SRM1), 0.25 wt% (i.e., SRM2), and 0.5 wt% (i.e., SRM3), respectively. To prepare the SRM herein, the rGO nanoparticles were dispersed in the solution of POSS(MEO_2MA-co-OEGMA) [20% (wt/vol)] in tetrahydrofuran (THF), which was then dried at room temperature overnight to evaporate the solvent. According to the visual observation (Fig. 2*A*), the SRM1 was transparent, but the SRM2 and SRM3 were black due to the presence of rGO nanoparticles (25). With a lower content of rGO in the SRM2, there were still some transparent spots in the membrane, where almost no rGO nanoparticles were present. Most of the area in the SRM3 membrane, however, turned out to be black due to the homogenous and denser distribution of rGO nanoparticles. Under the fabrication conditions of the SRM3, rGO nanoparticles appeared to also be homogeneously distributed in the membrane at a microscopic level (*SI Appendix*, Fig. S2*A*). Regardless of rGO incorporation, all membranes exhibited a similar surface morphology (*SI Appendix*, Fig. S2*B*), and their Fourier transfer infrared (FT-IR) spectral features were almost the same, without any peak shifts (*SI Appendix*, Fig. S2*C*). According to the differential scanning calorimetry (DSC) thermograms (Fig. 2*B*), the endotherm with the SRM1 was clearly observed at around 87 °C, which could be assigned as the melting temperature of the POSS(MEO_2MA-co-OEGMA), and this temperature was not changed for the SRM2 and SRM3 with rGO nanoparticles. Those results suggest that the addition of rGO did not affect the major characteristics of the polymer in the membrane.

As shown in Table 1, all SRMs prepared herein showed similar thicknesses; however, only the SRM3 could be ruptured properly and, as a consequence, fully open a drug reservoir when irradiated with NIR light under the conditions employed in this work (intensity, 8.85 W cm^{-2}; duration, 5 s) (*SI Appendix*, Fig. S2*D*). During NIR irradiation at the same dose, the temperature indeed increased, which was more dramatic as the rGO content increased, as shown in Fig. 2*C*. For the SRM1 without rGO, there was no temperature response upon NIR irradiation, as expected. The dimensional stability was also evaluated by assessing the thermal expansion behavior of the SRM. As shown in Fig. 2*D*, a dramatic decrease in thermal expansion coefficient (TEC) was observed with the addition of rGO, implying that the two-dimensional structure of rGO nanoparticles effectively restricted the mobility of polymer chains (30). Due to such a big difference in the TECs between intact polymer and polymer-rGO hybrid (Table 1), it is not that surprising why the membrane rupture occurs effectively in the case of SRM3. Those results could explain the more effective perforation of the SRM3 upon NIR irradiation: The SRM3 contained twice the amount of rGO, with a more homogeneous distribution, allowing for more effective heat generation without an obvious change in thermal expansion property, compared with the SRM2. According to the in vitro cytotoxicity evaluation with L929 cells, the membranes herein did not appear to release cytotoxic substances after rupturing via NIR irradiation

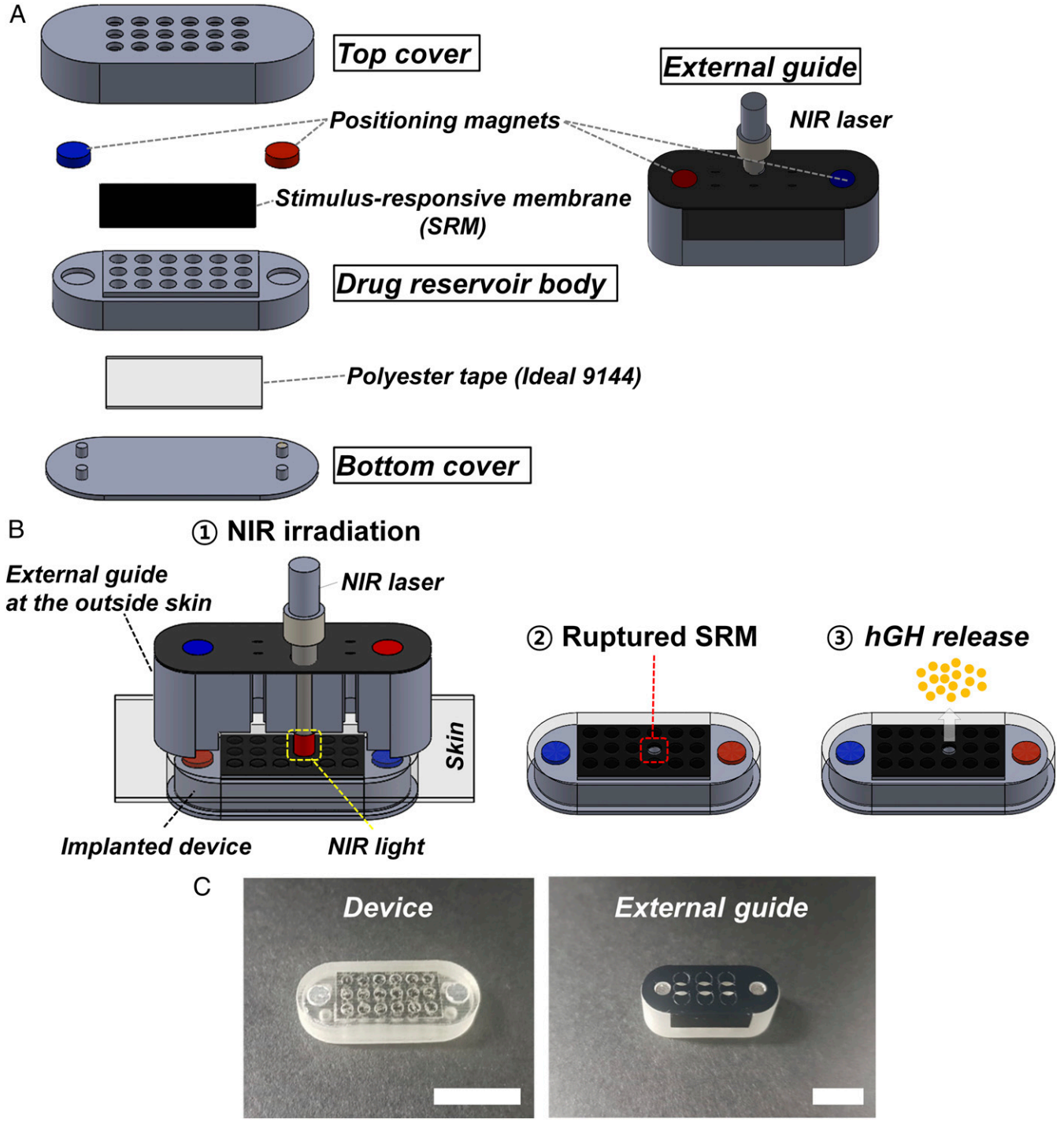

Fig. 1. Description of the device and external guide. (*A*) Three-dimensional schematic of the device and external guide (Solidworks; Dassault Systems). The composing units were each fabricated with a rapid prototyping PolyJet 3D printer (Eden 350V; Objet Geometries) using polyurethane copolymer (Fullcure 720 photopolymer), which were then assembled and seamlessly attached with medical epoxy (Epo-Tek 301; Epoxy Technology). A more detailed description of the device fabrication procedure is provided in *SI Appendix*, Fig. S1. (*B*) Working principle of the device: ① the NIR light is irradiated through the external guide aligned with the implanted device; ② the SRM capped on the selected drug reservoir is ruptured and opened; and ③ the hGH is released. (*C*) Optical images of the device and external guide. (Scale bar: 1 cm.)

(*SI Appendix*, Fig. S3). This could be ascribed to a very low exposure of the rGO nanoparticles expected from a whole device herein (~0.013 mg), which was much smaller than the rGO dose (7 mg·kg^{-1}) showing negligible toxicity in the previous study (31). The rGO nanoparticles freed from the device would be cleared mainly via the renal route (32).

In Vitro Drug Release Performance. Given the results above, we prepared the device using the SRM3 membrane, which exhibited the highest rupturing efficiency among the tested SRMs, and carried out in vitro drug release studies to assess its performance. As shown in Fig. 3, the device released hGH only at the times of NIR irradiation, with a high reproducibility (18.9 ± 1.31 μg per

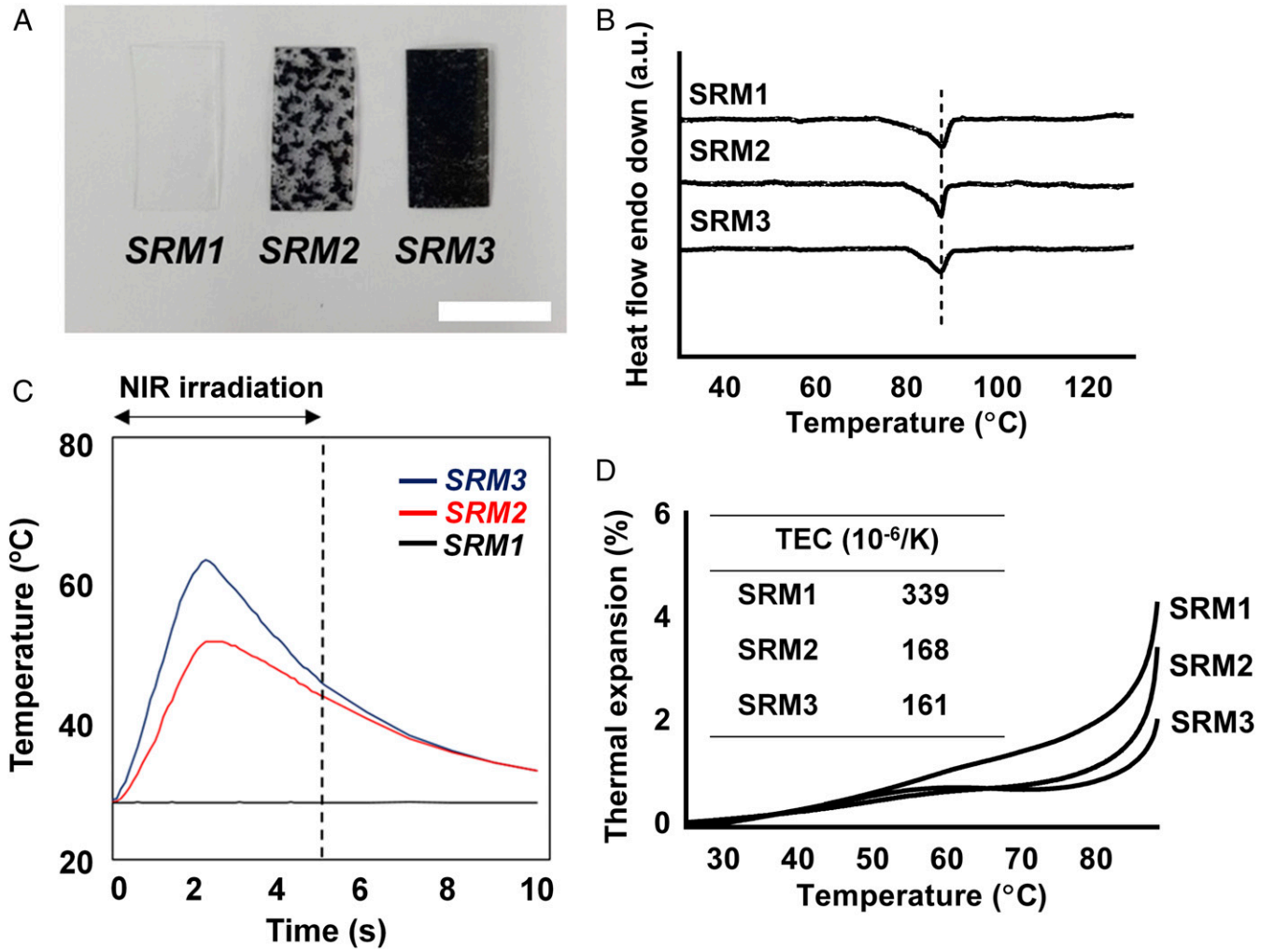

Fig. 2. Characterization of the rupturable SRMs. (*A*) Optical images. (Scale bar: 10 mm.) (*B*) DSC thermograms. (*C*) Temperature profiles during NIR light irradiation. (*D*) Profiles of thermal expansion behavior. The *Inset* table shows the thermal expansion coefficients (TECs) of the SRMs.

irradiation). Thus, during the period of no irradiation, no drug leakage was observed. After NIR irradiation, more than 80% of the hGH in the reservoir was released within 30 min, with almost complete release within 1 h (*SI Appendix*, Fig. S4), which could have been due to the relatively rapid rupture of the SRM3. During the whole testing period, the stability of hGH was well maintained when stored in the drug reservoirs of the device at 37 °C (*SI Appendix*, Fig. S5).

In Vivo Evaluation. To test the in vivo efficacy of hGH delivery, we employed hypophysectomized rats as an animal model with growth hormone deficiency (33). In this animal model, we implanted the device in a s.c. space and irradiated it with NIR light on the outside skin once per day for 14 d after implantation (i.e., the device group). For comparison, we also treated an animal group with a s.c. injection of an aqueous solution of hGH with the same dose and administration schedule (i.e., the s.c. injection group), as well as a group without treatment as the control group. To assess the pharmacokinetic and pharmacodynamic profiles, we measured the hGH and insulin-like growth factor (IGF1) concentrations in blood plasma at scheduled times after hGH administration, respectively (33, 34). IGF-I in serum is a pharmacodynamic marker in hGH administration, and therefore used in the present in vivo study, since the hGH protein could trigger a stimulation to produce IGF1 into systemic circulation (34).

We first assessed the short-term profiles of pharmacokinetics and pharmacodynamics with the s.c. injection and device animal groups (Fig. 4 *A* and *B*). After NIR irradiation through the external guide located on the skin, the hGH was indeed measured in blood plasma with the device group, indicating the release of hGH through the opened SRM on the drug reservoir. There was a slight difference in the time when the maximum hGH concentration in plasma was observed (T_{max}), which were 90 and 60 min with the device and s.c. injection groups, respectively. This could have been due to a slightly slow dissolution of hGH from the device (*SI Appendix*, Fig. S4) compared with the instantaneous exposure of a bolus of hGH via s.c. injection. However, the overall profile and, more importantly, the area

Table 1. Properties of SRM

	rGO contents, wt%	Thickness, μm	Rupturing degree*
SRM1	0	118 ± 8	None
SRM2	0.25	120 ± 7	Partial
SRM3	0.50	123 ± 5	Full

*Rupturing degree was evaluated via visual observation of the SRM after NIR irradiation (*SI Appendix*, Fig. S2*D*).

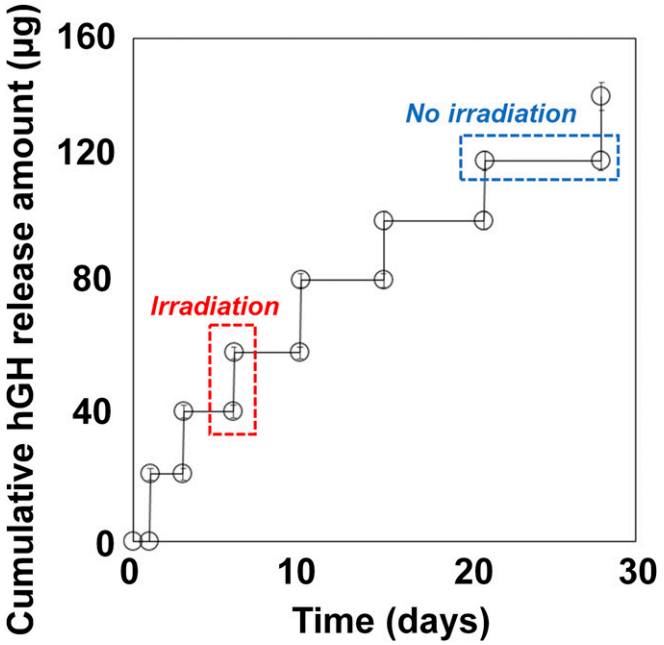

Fig. 3. In vitro hGH release profile of the device. The device was irradiated at scheduled times of 1, 3, 6, 10, 15, 21, and 28 d while being fully immersed in PBS (pH 7.4) at 37 °C (n = 5). Error bars are SD.

under the curve (AUC) of plasma hGH concentration versus time were not very different between the two groups (Fig. 4*A* and Table 2). Therefore, the pharmacodynamic profiles of both groups were also not very different: the IGF1 concentrations in plasma were 270.5 ± 36.8 and 261.1 ± 46.7 ng·mL^{-1} at 480 min in the device and s.c. injection groups, respectively ($P > 0.05$) (Fig. 4*B*).

We also examined the performance of the implanted device for a long-term period of 14 d. For pharmacokinetic analysis, the maximum hGH plasma concentrations were evaluated, and thus blood was obtained at 90 and 60 min after hGH administration on days 2, 7, and 14 in the device and s.c. injection groups, respectively. For pharmacodynamic analysis, the IGF1 plasma concentration was examined in the blood obtained at 480 min after hGH administration on days 2, 7, and 14 in both animal groups. As shown in Fig. 4 *C* and *D*, both hGH and IGF1 plasma concentrations were not different between the s.c. injection and device groups at any tested time, and they were statistically significantly higher than those measured in the control group ($P < 0.05$). Therefore, as shown in Fig. 4*E*, progressive weight gain, one of the representative parameters indicating growth (33), was observed in both device and s.c. injection groups with a high similarity, while there was no increase in body weight in the control group. When the blood samples were collected from the device group on days 4 and 10 right before NIR irradiation (i.e., at times without NIR irradiation) (*SI Appendix*, Fig. S6), hGH plasma concentrations were very low (3.49 ± 0.31 ng·mL^{-1}), which were not statistically significantly different from those for the control group without treatment (2.74 ± 0.21 ng·mL^{-1}) ($P > 0.05$), indicating the leak-proof property of the device. Therefore, the results suggest that the device herein could indeed deliver hGH similarly effectively as done with the conventional s.c. injection.

Histopathology. To assess in vivo biocompatibility, the tissues around the device were biopsied at the end point of experiments (14 d after implantation) from the device group and evaluated histologically by hematoxylin and eosin (H&E) staining. As shown in Fig. 5, the tissues did not exhibit any sign of injury after repetitive NIR irradiation, although a mild inflammatory response was observed at the site adjacent to the device. The surrounding tissue of the device showed the formation of fibrous capsules, which was also observed with many other implanted systems (11, 35). We also collected blood from the device group at the end point of experiments to measure inflammatory markers in blood plasma, such as tumor necrosis factor (TNF)-α, interleukin (IL)-1b, and IL-6. All were within a normal range at 14 d after device implantation (*SI Appendix*, Table S1).

Discussion

To mimic circadian rhythms, many drugs need to be delivered in on-demand and pulsatile manners (36, 37). For this purpose, such drugs are often prescribed to be administered by multiple needle injections (38–40), which could cause poor patient compliance. One way to resolve this is with implantable devices enabled with on-demand and pulsatile drug delivery (3). To achieve such delivery profiles, however, the devices often contain the active driving units and their power source, i.e., battery, in addition to the drug reservoirs (4–11), making them overly bulky and heavy for implantation. For the implantable drug delivery devices in clinical use, those active units occupy more than 80% of the device volume (11, 41).

Therefore, in this work, we have proposed an implantable device equipped with multiple drug reservoirs, and most importantly, the reservoirs were capped with a stimulus-responsive hybrid membrane (SRM). Through this SRM, therefore, we aimed to open a drug reservoir only at the needed time by a noninvasive means, such as NIR irradiation from the outside body (42), thereby providing on-demand and pulsatile drug administration without an internal driving unit. Our findings revealed that the SRM3, composed of POSS(MEO_2MA-co-OEGMA) with an rGO content of 0.5 wt%, could be effectively ruptured to fully open a drug reservoir with a low energy of NIR light (8.85 W·cm^{-2} for 5 s) (Table 1 and *SI Appendix*, Fig. S2*D*). With the presence of a photothermal rGO nanoparticles, the temperature of SRM3 was indeed increased upon NIR irradiation (Fig. 2*C*), which in turn shrank and tore a constituent material of a thermosensitive polymer, POSS(MEO_2MA-co-OEGMA), capped on the drug reservoir. As the rGO nanoparticles possessed a more efficient photothermal property than the graphene oxide (GO) nanoparticles (*SI Appendix*, Fig. S7*D*), we prepared SRM3 to be composed mainly of a seamless polymer with a low content of rGO nanoparticles to prevent drug leakage while there was no NIR irradiation (Fig. 3).

Therefore, with an external guide proposed in this work (Fig. 1), an NIR light could be aligned and irradiated selectively at the SRM3 on each of the targeted drug reservoirs to release drug reproducibly in a pulsatile manner (Fig. 3). Our in vivo experiments with hGH further confirmed that the hGH in the device after implantation was released after NIR irradiation onto the outside skin, and due to a relatively rapid dissolution of hGH from the opened drug reservoir, its pharmacokinetic and pharmacodynamic profiles were not significantly different from those of the s.c. injected bolus hGH (Fig. 4 *A* and *B*). During the whole testing period of 14 d in this work, the device administered hGH reproducibly and similarly to multiple daily injections (Fig. 4 *C* and *D*). Hence, both the device and s.c. injection groups of growth hormone-deficient animal models exhibited a similar progressive weight gain (Fig. 4*E*).

Those results suggest that, after one-time implantation, the device herein could deliver hGH noninvasively while maintaining its standardized clinical regimen. In that respect, our device could also be applied to other drugs needing on-demand and pulsatile delivery, such as parathyroid hormone (40) and alirocumab (39). In current clinical settings, the hGH is often prescribed to be injected three times per week for a year for treatment of

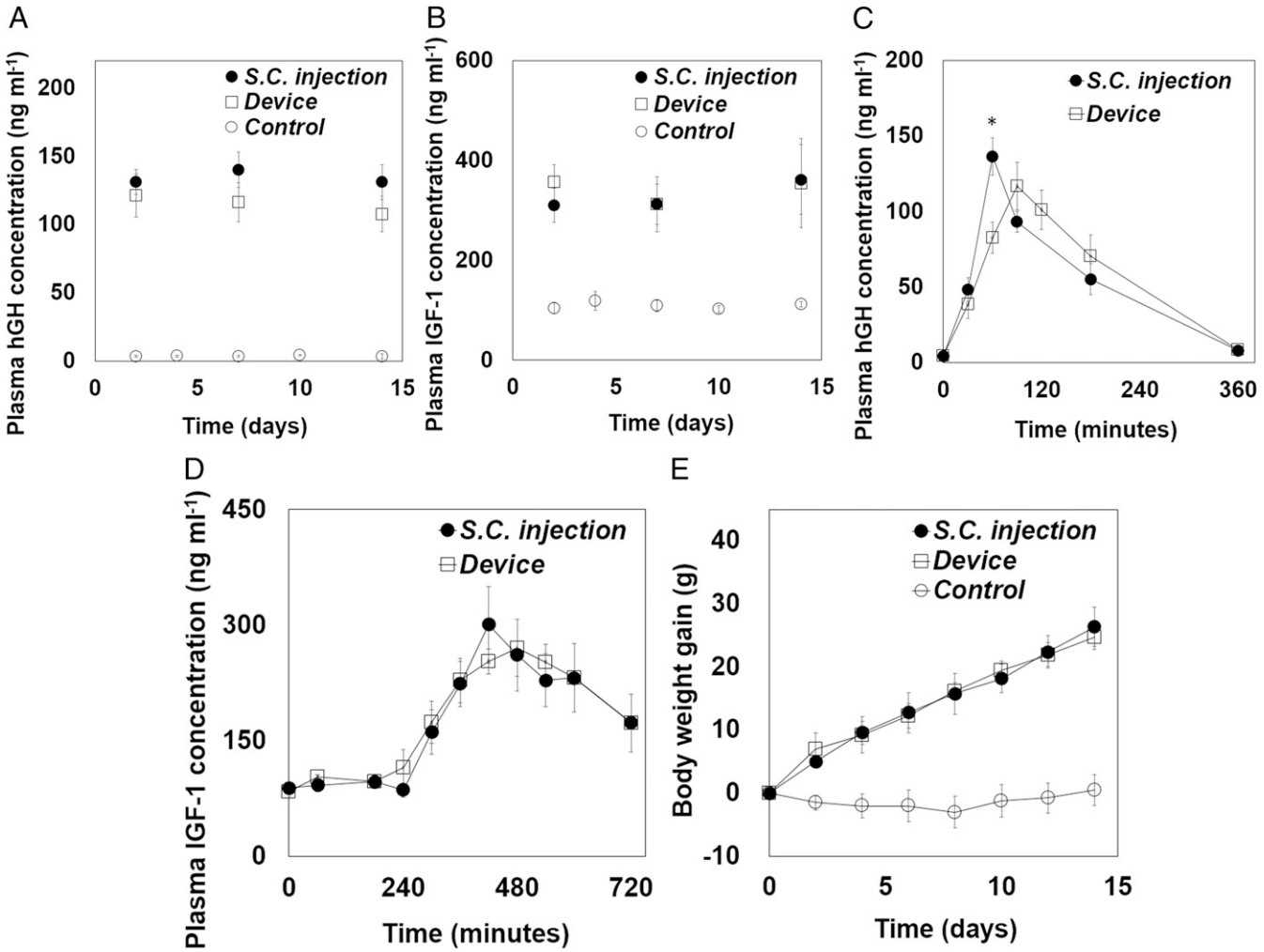

Fig. 4. In vivo efficacy profiles of hGH delivery. (*A*) Profiles of plasma hGH concentration measured from the blood sampled at −1, 30, 60, 90, 120, 180, and 360 min after hGH administration. The maximum hGH concentration was measured at 60 and 90 min in the s.c. injection ($n = 4$) and device ($n = 4$) groups, respectively. Error bars are SD. The areas under the curve of plasma hGH concentration versus time (AUC) in the device group and s.c. injection group were 20,910 ± 2,539 and 17,173 ± 1,852 ng·mL^{-1}·min^{-1}, respectively, which were not statistically significantly different ($P > 0.05$). The AUC was calculated by using the trapezoidal rule. Asterisk indicates statistically significant difference between the two groups ($P < 0.05$). (*B*) Profiles of plasma IGF1 concentration measured from the blood sampled at −1, 60, 180, 240, 300, 360, 420, 480, 540, 600, and 720 min after hGH administration. The IGF1 concentrations measured at 480 min were similar between the s.c. injection ($n = 4$) and device ($n = 4$) groups. Error bars are SD. Long-term profiles of (*C*) hGH and (*D*) IGF1 concentration in plasma measured from the blood sampled after hGH administration on days 2, 7, and 14 in the s.c. injection ($n = 4$) and device ($n = 4$) groups. For the control group ($n = 4$), the blood was withdrawn on days 2, 4, 7, 10, and 14. Error bars are SD. (*E*) Profiles of body weight gain measured every 2 d for the whole testing period of 14 d. Error bars are SD.

growth hormone deficiency in pediatric patients (38, 43). Alirocumab, a drug for hypercholesterolemia, is given at least once every 2 wk for at least a year (39). In addition, parathyroid hormone for treatment of osteoporosis requires intermittent administrations of drug every day for at least a year (40, 44). In this regard, the device may need to contain at least 360 drug reservoirs, and this would increase the dimension and weight of the device to ∼9.5 mL (i.e., 70 mm × 27 mm × 5 mm, L × W × H) and 8 g, respectively (*SI Appendix*, Fig. S8), which would, notably, still be smaller than the implantable drug delivery devices already in clinical use (∼120 mL and ∼165 g) (41).

Previously, an implantable device with multiple drug reservoirs was made fully of a biocompatible polymer (45), where each of the reservoirs was sealed with a polymeric stopper for preprogrammed, pulsatile drug delivery. The device could be designed to be compact without any electronic components; however, the device was not based on patient-driven, on-demand drug release. The implantable devices to trigger drug release by NIR irradiation were proposed for on-demand drug release (15, 46). However, to allow for a meaningful increase in drug release, those devices needed a relatively long time of NIR irradiation (∼20 min). As the drug was not encased in the reservoir but rather loaded in a body of the device itself, continuous drug release, albeit small, was observed during no-NIR irradiation periods. Therefore, the device proposed in this work can be considered advantageous as it is abled with both pulsatile and

Table 2. Pharmacokinetic parameters of hGH

Parameter	Device group	s.c. injection group
C_{max}, ng·mL^{-1}	117 ± 15	136 ± 12
T_{max}, min	90	60
AUC, ng·min·mL^{-1}	20,910 ± 2,539	17,173 ± 1852

The area under the plasma concentration-time curve (AUC) was calculated by using the trapezoidal rule (56).

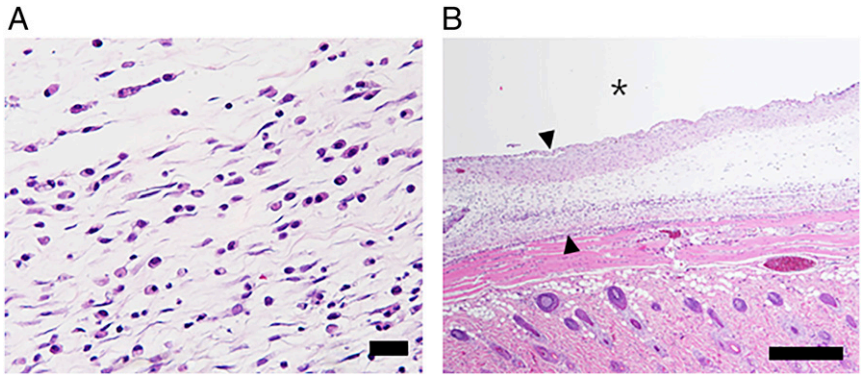

Fig. 5. Representative image of the hematoxylin and eosin (H&E)-stained tissues around the implanted device. The degree of inflammatory response was evaluated on H&E-stained tissues biopsied at the end point of experiments (14 d after implantation). The images were acquired at (*A*) 200× and (*B*) 50× magnifications for evaluation of inflammation and capsule thickness, respectively. The asterisk (*) indicates the location of the implanted device. The arrows indicate the capsule formed around the implanted device. (Scale bars: *A*, 200 μm; *B*, 500 μm.)

on-demand drug delivery without any electronic components inside. Moreover, with the use of a SRM hybridized with a thermosensitive polymer and photothermal rGO nanoparticles, our device can rupture the membrane with a relatively short time of NIR irradiation (~5 s), thereby allowing for pulsatile drug release only at the needed times. As the membrane can seamlessly seal each of the drug reservoirs in the device, there is no drug leakage during no-NIR irradiation periods (*SI Appendix*, Fig. S6).

In this work, we suggested an external guide as a prototype for alignment of NIR irradiation onto a specific, single-drug reservoir. Although a specific drug reservoir in the implanted device could still be properly selected without errors, an external guide equipped with proper software and electronics can be more advantageous, considering the device usability and convenience for the patients. For example, an external guide can be designed to store the administration history, including the one of the already-used drug reservoirs (47) and it may also contain the hardware abled with NIR irradiation, as well as wireless communications with a mobile device, to further enhance the usability of the system herein (48, 49). To be operable, such an external guide may need a battery, which, however, can be easily replaced as it is purposed to be used outside of the body.

In summary, we have proposed an implantable multireservoir device with an SRM for on-demand and pulsatile delivery of hGH. Multiple drug reservoirs in the device can each be loaded with the same amount of hGH and seamlessly capped with the SRM. Due to the high photothermal property of rGO, the SRM can be made mainly of POSS(MEO_2MA-co-OEGMA) with a low content of rGO nanoparticles. Under this condition, the SRM can still be ruptured to open each of the selected drug reservoirs and release hGH reproducibly in response to short, noninvasive NIR irradiation, and there is no hGH leakage during no NIR irradiation. Our in vivo experimental results reveal that the implanted device herein could deliver hGH only when NIR irradiation is applied from the outside body, and the pharmacokinetic and pharmacodynamic profiles were similar to those of s.c. injected hGH. Therefore, we conclude that the device herein can be a promising, minimally invasive strategy for on-demand and pulsatile drug delivery.

Materials and Methods

Synthesis of POSS(MEO_2MA-co-OEGMA). We prepared POSS(MEO_2MA-co-OEGMA) as a thermosensitive polymer for the SRM in this work, following a previous protocol with slight modifications (27, 50), where 2-(2-methoxyethoxy) ethyl methacrylate (MEO_2MA), oligo(ethylene glycol) methacrylate (OEGMA), and acryloisobutyl polyhedral oligomeric silsesquioxane (POSS) were polymerized with azobisisobutyronitrile (AIBN) as initiator (*SI Appendix*, Fig. S9*A*). For this, 13.4 g (71.3 mmol) of MEO_2MA, 4.4 g (9.25 mmol) of OEGMA, 18.9 g (20.02 mmol) of POSS, and 0.16 g (0.974 mmol) of AIBN were added to a Schlenk flask containing 116 mL of THF. The freeze–pump–thaw cycle was repeated three times to degas the mixture. After that, the reaction mixture was stirred at 65 °C for 12 h, which was then diluted with deionized water for 12 h and subsequently purified by dialysis (Roth; ZelluTrans membrane; MW cutoff, 4,000–6,000) against deionized water to remove the unreacted MEO_2MA and OEGMA monomers. After drying for 12 h, the purified POSS(MEO_2MA-co-OEGMA) was obtained. ^{1}H NMR and FT-IR spectra (*SI Appendix*, Fig. S9 *B* and *C*) confirmed the successful fabrication of POSS(MEO_2MA-co-OEGMA) in this work (27).

Synthesis of rGO Nanoparticles. To prepare rGO nanoparticles, we first synthesized the GO by oxidation of graphite powder according to the Hummers method with slight modifications (51). To obtain the exfoliated GO solution, 0.2 g of GO was dispersed in 200 mL of deionized water under sonication for 1 h. The obtained brown colloidal solution was then centrifuged under a condition of 4,000 rpm for 20 min to remove any aggregates or unexfoliated materials. The exfoliated GO colloidal solution was then sealed in a Teflon-lined autoclave for hydrothermal reaction at 180 °C for 6 h and freeze-dried to produce rGO nanoparticles. The product from each reaction step (i.e., graphite, GO, and rGO) was monitored by X-ray diffraction, FT-IR spectroscopy, and UV-vis spectroscopy (*SI Appendix*, Fig. S7 *A–F*) to confirm successful fabrication of rGO (52). The rGO nanoparticles herein exhibited a favorable light-to-heat conversion property, facilitating its photothermal application in the SRM (*SI Appendix*, Fig. S7*G*).

Characterizations. The X-ray diffraction patterns for graphite, GO, and rGO were recorded using a diffractometer (RINT-Ultima III; Rigaku) with Ni-filtered Cu-Kα radiation (λ = 1.5418 Å) operated at 40 kV and 30 mA. For FT-IR spectroscopic analysis, all of the carbon samples, including polymer and SRMs, were prepared on the basis of the standard KBr disk method and measured with a JASCO FT-IR 6100 spectrometer (JASCO). ^{1}H NMR data for the present POSS(MEO_2MA-co-OEGMA) was obtained by a Bruker DRX-500 NMR spectrometer (Bruker) with deuterated chloroform as solvent. The morphologies for SRMs were observed via field-emission scanning electron microscopy (JSM-6700F; JEOL) and transmission electron microscopy (JEM-2100F; JEOL). DSC (DSC 8000; Perkin-Elmer) was used to obtain the thermograms of SRMs at a ramp rate of 5 °C·min^{-1}. Their temperature profiles were recorded using an infrared thermometer (Optris LaserSight; Optris) upon NIR irradiation (808 nm, 8.85 W·cm^{-2}) through a freshly obtained rat tissue with a thickness of 1–1.5 mm on each SRM. The thermal expansion behaviors of SRMs were assessed with a thermomechanical analyzer (TMA 402 F3; NETZSCH) at a ramp rate of 5 °C·min^{-1}.

In Vitro Drug Release Tests. The in vitro drug release experiment was performed while the device was fully immersed in PBS (pH 7.4) at 37 °C. The device was irradiated at 1, 3, 6, 10, 15, 21, and 28 d by applying the tip of the NIR laser through the external guide that was aligned with the device, at a gap of 1 mm, to simulate the skin after implantation (53). After irradiation, the aliquot was collected and measured to check the hGH concentration, using an Agilent 1260 series HPLC system equipped with a UV detector set at 210 nm and a reversed-phase column (250 mm × 4.6 mm; pore, 5 μm; Vydac214ATP54;

Agilent Technology). The mobile phase was made by mixing 0.05 M Tris buffer (pH 7.5) and n-propanol [67:33 (vol/vol)]. The flow rate and column temperature were set at 0.5 mL·min^{-1} and 45 °C, respectively (54).

In Vivo Experiments. All in vivo experimental protocols were approved by the Institutional Animal Care and Use Committee (IACUC no. 17-0017-C1A0) at Seoul National University Hospital Biomedical Research Institute. Male hypophysectomized rats, weighing 90–100 g, were housed under a 12/12-h light/dark cycle and were provided with food and water ad libitum. In this work, we employed three different animal groups, i.e., the device, s.c. injection, and control groups. For the device group, the device was implanted in a s.c. space, as described in *SI Appendix*, Fig. S10. For pharmacokinetic and pharmacodynamic analysis, 0.3 mL of blood was withdrawn from the lateral tail vein, which was then immediately centrifuged at 3,000 × *g* for 15 min at 4 °C to collect the plasma. The blood plasma was stored in the freezer at −20 °C before analysis. The plasma concentrations of hGH and IGF1 were quantified using the Human Growth Hormone Elisa Kit (Human Growth Hormone Quantikine ELISA Kit; R&D Systems) and IGF1 Elisa Kit (Mouse/Rat IGF1 Quantikine ELISA Kit; R&D Systems), respectively.

Histopathologic Evaluation. For histopathologic evaluation, the rats from the device group were killed by carbon dioxide inhalation at the end point of experiments (i.e., 14 d after implantation), and the dorsal region tissues around the implanted device were harvested. The resulting tissues were fixed in 4% paraformaldehyde in a conical tube for 24 h and embedded in paraffin wax. The paraffinized sample was then cut into 4-μm-thick slices to prepare the tissue slides. The slides were then stained with H&E. Finally, the stained slides were evaluated by a professional pathologist using an optical microscope (BX53; Olympus). We assessed the degree of inflammation based on the number of polymorphonuclear cells from a slide image of 0.48 mm^2 (200× magnification). Furthermore, we measured the thickness of the fibrotic capsule around the device from a slide image of 6.25 mm^2 (50× magnification), following the protocol in a previous work (55). Three images were analyzed from each of the four rats, and hence a total of 12 images was analyzed per animal group.

Statistical Analysis. All data for plasma hGH and IGF1 concentrations at each scheduled time were compared among the tested animal groups for statistical significance via nonparametric methods (Kruskal–Wallis ANOVA). $P < 0.05$ was considered statistically significant. The statistical software application used was SPSS (SPSS, version 22; IBM).

ACKNOWLEDGMENTS. This research was supported by the Basic Science Research Program through the National Research Foundation of Korea (NRF) funded by the Ministry of Science, ICT and Future Planning (2017R1A2B3004830) and the framework of the International Cooperation Program managed by NRF (2017K2A9A2A10013104).

1. N. M. Elman, U. M. Upadhyay, Medical applications of implantable drug delivery microdevices based on MEMS (micro-electro-mechanical-systems). *Curr. Pharm. Biotechnol.* **11**, 398–403 (2010).
2. N. M. Elman, H. L. Ho Duc, M. J. Cima, An implantable MEMS drug delivery device for rapid delivery in ambulatory emergency care. *Biomed. Microdevices* **11**, 625–631 (2009).
3. C. L. Stevenson, J. T. Santini , Jr, R. Langer, Reservoir-based drug delivery systems utilizing microtechnology. *Adv. Drug Deliv. Rev.* **64**, 1590–1602 (2012).
4. H. Gensler, R. Sheybani, P. Y. Li, R. L. Mann, E. Meng, An implantable MEMS micropump system for drug delivery in small animals. *Biomed. Microdevices* **14**, 483–496 (2012).
5. P. Y. Li *et al*., An electrochemical intraocular drug delivery device. *Sens. Actuators A Phys.* **143**, 41–48 (2008).
6. K. Junwu, Y. Zhigang, P. Taijiang, C. Guangming, W. Boda, Design and test of a high-performance piezoelectric micropump for drug delivery. *Sens. Actuators A Phys.* **121**, 156–161 (2005).
7. T. Tan, S. W. Watts, R. P. Davis, Drug delivery: Enabling technology for drug discovery and development. iPRECIO micro infusion pump: Programmable, refillable, and implantable. *Front. Pharmacol.* **2**, 44 (2011).
8. J. T. Santini, Jr, M. J. Cima, R. Langer, A controlled-release microchip. *Nature* **397**, 335–338 (1999).
9. Y. Li *et al*., In vivo delivery of BCNU from a MEMS device to a tumor model. *J. Control. Release* **106**, 138–145 (2005).
10. J. H. Prescott *et al*., Chronic, programmed polypeptide delivery from an implanted, multireservoir microchip device. *Nat. Biotechnol.* **24**, 437–438 (2006).
11. R. Farra, *et al*., First-in-human testing of a wirelessly controlled drug delivery microchip. *Sci. Transl. Med.* **4**, 122ra21 (2012).
12. S. Stauss, I. Honma, Biocompatible batteries—materials and chemistry, fabrication, applications, and future prospects. *Bull. Chem. Soc. Jpn.* **91**, 492–505 (2018).
13. R. Feiner, T. Dvir, Tissue–electronics interfaces: From implantable devices to engineered tissues. *Nat. Rev. Mater.* **3**, 17076 (2017).
14. J. Jackson, A. Chen, H. Zhang, H. Burt, M. Chiao, Design and near-infrared actuation of a gold nanorod–polymer microelectromechanical device for on-demand drug delivery. *Micromachines (Basel)* **9**, E28 (2018).
15. B. P. Timko *et al*., Near-infrared-actuated devices for remotely controlled drug delivery. *Proc. Natl. Acad. Sci. U.S.A.* **111**, 1349–1354 (2014).
16. T. Hoare *et al*., A magnetically triggered composite membrane for on-demand drug delivery. *Nano Lett.* **9**, 3651–3657 (2009).
17. F. N. Pirmoradi, J. K. Jackson, H. M. Burt, M. Chiao, On-demand controlled release of docetaxel from a battery-less MEMS drug delivery device. *Lab Chip* **11**, 2744–2752 (2011).
18. D. W. Dunstan *et al*., Breaking up prolonged sitting reduces postprandial glucose and insulin responses. *Diabetes Care* **35**, 976–983 (2012).
19. E. E. Müller, V. Locatelli, D. Cocchi, Neuroendocrine control of growth hormone secretion. *Physiol. Rev.* **79**, 511–607 (1999).
20. F. He *et al*., A new single 808 nm NIR light-induced imaging-guided multifunctional cancer therapy platform. *Adv. Funct. Mater.* **25**, 3966–3976 (2015).
21. R. Vankayala, C. L. Kuo, K. Nuthalapati, C. S. Chiang, K. C. Hwang, Nucleus-targeting gold nanoclusters for simultaneous in vivo fluorescence imaging, gene delivery, and NIR-light activated photodynamic therapy. *Adv. Funct. Mater.* **25**, 5934–5945 (2015).
22. X. Ding *et al*., Multifunctional core/satellite polydopamine@ Nd^{3+}-sensitized upconversion nanocomposite: A single 808 nm near-infrared light-triggered theranostic platform for in vivo imaging-guided photothermal therapy. *Nano Res.* **10**, 3434–3446 (2017).
23. Y. W. Chen, P. J. Chen, S. H. Hu, I. W. Chen, S. Y. Chen, NIR-triggered synergic photochemothermal therapy delivered by reduced graphene oxide/carbon/mesoporous silica nanocookies. *Adv. Funct. Mater.* **24**, 451–459 (2014).
24. S. H. Hu, Y. W. Chen, W. T. Hung, I. W. Chen, S. Y. Chen, Quantum-dot-tagged reduced graphene oxide nanocomposites for bright fluorescence bioimaging and photothermal therapy monitored in situ. *Adv. Mater.* **24**, 1748–1754 (2012).
25. H. L. Guo, P. Su, X. Kang, S. K. Ning, Synthesis and characterization of nitrogen-doped graphene hydrogels by hydrothermal route with urea as reducing-doping agents. *J. Mater. Chem. A* **1**, 2248–2255 (2013).
26. L. Li *et al*., Synthesis and self-assembly behavior of thermo-responsive star-shaped POSS–(PCL–P (MEO_2 MA-co-PEGMA)) 16 inorganic/organic hybrid block copolymers with tunable lower critical solution temperature. *New J. Chem.* **40**, 4761–4768 (2016).
27. W. Yuan, T. Shen, X. Liu, J. Ren, Star-shaped inorganic–organic hybrid polymers with polyhedral oligomeric silsesquioxane core: Synthesis, self-assembly and tunable thermoresponse. *Mater. Lett.* **111**, 9–12 (2013).
28. F. Roelfsema *et al*., Growth hormone (GH) secretion in patients with an inactivating defect of the GH-releasing hormone (GHRH) receptor is pulsatile: Evidence for a role for non-GHRH inputs into the generation of GH pulses. *J. Clin. Endocrinol. Metab.* **86**, 2459–2464 (2001).
29. M. Linder, S. Hüther, M. Reinacher, In vivo reactions in mice and in vitro reactions in feline cells to implantable microchip transponders with different surface materials. *Vet. Rec.* **165**, 45–50 (2009).
30. S. Wang, M. Tambraparni, J. Qiu, J. Tipton, D. Dean, Thermal expansion of graphene composites. *Macromolecules* **42**, 5251–5255 (2009).
31. M. C. P. Mendonça *et al*., Reduced graphene oxide: Nanotoxicological profile in rats. *J. Nanobiotechnology* **14**, 53 (2016).
32. L. Ou *et al*., Toxicity of graphene-family nanoparticles: A general review of the origins and mechanisms. *Part. Fibre Toxicol.* **13**, 57–81 (2016).
33. M. R. Park, B. B. Seo, S. C. Song, Dual ionic interaction system based on polyelectrolyte complex and ionic, injectable, and thermosensitive hydrogel for sustained release of human growth hormone. *Biomaterials* **34**, 1327–1336 (2013).
34. N. K. Singh, Q. V. Nguyen, B. S. Kim, D. S. Lee, Nanostructure controlled sustained delivery of human growth hormone using injectable, biodegradable, pH/temperature responsive nanobiohybrid hydrogel. *Nanoscale* **7**, 3043–3054 (2015).
35. S. H. Lee *et al*., Implantable small device enabled with magnetic actuation for on-demand and pulsatile drug delivery. *J. Control. Release* **286**, 224–230 (2018).
36. M. H. Smolensky, N. A. Peppas, Chronobiology, drug delivery, and chronotherapeutics. *Adv. Drug Deliv. Rev.* **59**, 828–851 (2007).
37. B. B. C. Youan, Chronopharmaceutics: Gimmick or clinically relevant approach to drug delivery? *J. Control. Release* **98**, 337–353 (2004).
38. S. M. de Muinck Keizer-Schrama *et al*.; Dutch Growth Hormone Working Group, Dose-response study of biosynthetic human growth hormone (GH) in GH-deficient children: Effects on auxological and biochemical parameters. *J. Clin. Endocrinol. Metab.* **74**, 898–905 (1992).
39. G. G. Schwartz *et al*., Effect of alirocumab, a monoclonal antibody to PCSK9, on long-term cardiovascular outcomes following acute coronary syndromes: Rationale and design of the ODYSSEY outcomes trial. *Am. Heart J.* **168**, 682–689 (2014).
40. D. W. Dempster *et al*., Effects of daily treatment with parathyroid hormone on bone microarchitecture and turnover in patients with osteoporosis: A paired biopsy study. *J. Bone Miner. Res.* **16**, 1846–1853 (2001).
41. A. Buvanendran, S. Diwan, T. Deer, *Intrathecal Drug Delivery for Pain and Spasticity E-Book: A Volume in the Interventional and Neuromodulatory Techniques for Pain Management Series* (Elsevier Health Sciences, 2011).
42. S. Kim, J. Cho, J. Choi, D. H. Lee, J. K. Kim, Characterization of porcine tissue perforation using high-power near-infrared laser at 808-nm wavelength. *Trans. Korean Soc. Mech. Eng. B* **37**, 807–814 (2013).
43. V. H. Koch *et al*., Accelerated growth after recombinant human growth hormone treatment of children with chronic renal failure. *J. Pediatr.* **115**, 365–371 (1989).

44. C. P. Jerome, D. B. Burr, T. Van Bibber, J. M. Hock, R. Brommage, Treatment with human parathyroid hormone (1-34) for 18 months increases cancellous bone volume and improves trabecular architecture in ovariectomized cynomolgus monkeys (*Macaca fascicularis*). *Bone* **28**, 150–159 (2001).
45. A. C. Richards Grayson *et al*., Multi-pulse drug delivery from a resorbable polymeric microchip device. *Nat. Mater.* **2**, 767–772 (2003).
46. M. S. Yavuz *et al*., Gold nanocages covered by smart polymers for controlled release with near-infrared light. *Nat. Mater.* **8**, 935–939 (2009).
47. S. H. Lee *et al*., Wirelessly controlled implantable system for on-demand and pulsatile insulin administration. *Sci. Rep.* **9**, 5009 (2019).
48. O. El-Gayar, P. Timsina, N. Nawar, W. Eid, Mobile applications for diabetes self-management: Status and potential. *J. Diabetes Sci. Technol.* **7**, 247–262 (2013).
49. N. Ramanathan, D. Swendeman, W. S. Comulada, D. Estrin, M. J. Rotheram-Borus, Identifying preferences for mobile health applications for self-monitoring and self-management: Focus group findings from HIV-positive persons and young mothers. *Int. J. Med. Inform.* **82**, e38–e46 (2013).
50. N. Fechler, N. Badi, K. Schade, S. Pfeifer, J. F. Lutz, Thermogelation of PEG-based macromolecules of controlled architecture. *Macromolecules* **42**, 33–36 (2008).
51. W. S. Hummers , Jr, R. E. Offeman, Preparation of graphitic oxide. *J. Am. Chem. Soc.* **80**, 1339 (1958).
52. K. S. Novoselov *et al*., Electric field effect in atomically thin carbon films. *Science* **306**, 666–669 (2004).
53. H. Takeuchi *et al*., Influence of skin thickness on the in vitro permeabilities of drugs through Sprague-Dawley rat or Yucatan micropig skin. *Biol. Pharm. Bull.* **35**, 192–202 (2012).
54. S. J. Kim, S. K. Hahn, M. J. Kim, D. H. Kim, Y. P. Lee, Development of a novel sustained release formulation of recombinant human growth hormone using sodium hyaluronate microparticles. *J. Control. Release* **104**, 323–335 (2005).
55. S. Park *et al*., Acute suppression of TGF-ß with local, sustained release of tranilast against the formation of fibrous capsules around silicone implants. *J. Control. Release* **200**, 125–137 (2015).
56. W. L. Chiou, Critical evaluation of the potential error in pharmacokinetic studies of using the linear trapezoidal rule method for the calculation of the area under the plasma level–time curve. *J. Pharmacokinet. Biopharm.* **6**, 539–546 (1978).